ENVIRONMENTAL RESEARCH
LETTERS

LETTER • OPEN ACCESS

2020/21 record-breaking cold waves in east of China enhanced by the ‘Warm Arctic-Cold Siberia’ pattern

ENVIRONMENTAL RESEARCH
LETTERS

LETTER

2020/21 record-breaking cold waves in east of China enhanced by the 'Warm Arctic-Cold Siberia' pattern

Yijia Zhang[1], Zhicong Yin[1,2,3,*], Huijun Wang[1,2,3] and Shengping He[1,4]

[1] Key Laboratory of Meteorological Disaster, Ministry of Education/Joint International Research Laboratory of Climate and Environment Change (ILCEC)/Collaborative Innovation Center on Forecast and Evaluation of Meteorological Disasters (CIC-FEMD), Nanjing University of Information Science & Technology, Nanjing 210044, People's Republic of China
[2] Southern Marine Science and Engineering Guangdong Laboratory (Zhuhai), Zhuhai, People's Republic of China
[3] Nansen-Zhu International Research Centre, Institute of Atmospheric Physics, Chinese Academy of Sciences, Beijing, People's Republic of China
[4] Geophysical Institute, University of Bergen and Bjerknes Centre for Climate Research, Bergen, Norway
[*] Author to whom any correspondence should be addressed.

E-mail: yinzhc@163.com

Keywords: extreme climate, Arctic warming, Eurasia cooling, cold wave, temperature

Supplementary material for this article is available online

OPEN ACCESS

RECEIVED
15 May 2021

REVISED
17 August 2021

ACCEPTED FOR PUBLICATION
19 August 2021

PUBLISHED
2 September 2021

Abstract

Extreme cold waves frequently occur in east of China that dramatically endanger ecological agriculture, power infrastructure and human life. In this study, we found that the 'Warm Arctic-Cold Siberia' pattern (WACS) significantly enhanced cold waves in east of China according to daily composites from 1979 to 2018. During the winter 2020/21, a record-breaking cold wave broke out following a noticeable WACS phenomenon and induced the record-low surface air temperature at 60 meteorological stations since they were established (nearly 60 years). On 3 January 2021, the difference in temperature anomaly between the Barents–Kara Sea and Siberia reached 20 °C, the peak of winter 2020/21. With a shrinking meridional temperature gradient, the atmospheric baroclinicity weakened correspondingly. The accompanying atmospheric anomalies, i.e. the persistent Ural Blocking High and Baikal deep trough effectively transported stronger cold air than the sole impact from Arctic warming. After 4 d, the east of China experienced a severe surface air temperature decrease of more than 8 °C, covering an area of 2500 000 km^2. During the same winter, a record-breaking warm event occurred in February 2021, and the 'Cold Arctic-Warm Eurasia' pattern also appeared as a precursory signal. Furthermore, on the interannual scale, the connection between winter-mean temperature anomalies in east of China and the WACS pattern also existed and even performed more strongly in both observations and simulation data of CMIP6.

1. Introduction

Extreme cold waves are disastrous weather events that have destructive effects on agriculture, transportation, power infrastructure, and human health (Cohen *et al* 2014, Ding *et al* 2020). Accumulating evidence indicates that extreme cold waves in east of China (EC; 25°–40° N, 105°–120° E) have become more serious and frequent under the global warming (Ding *et al* 2008, Luo *et al* 2020). In January 2016, a supercold wave occurred in EC (Ma and Zhu 2019), with a surface air temperature (SAT) decrease of more than 12 °C over an area of 1764 000 km^2. The proximate causes were an extremely strong Ural Blocking High (UBH) and a record-breaking Siberian High (SH; Ma and Zhu 2019). In addition, a large-scale persistent low-temperature anomaly appeared in mid-late January 2018 accompanied by two large-scale heavy snowfall events, which were also caused by the frequent southward invasion of polar cold air under the guidance of the strengthened SH (Sun *et al* 2019). More recently, a record-breaking extreme cold wave invaded EC in late December and early January in the winter of 2020 with two cold air outbreaks on the 28–31 December 2020 and 5–8 January 2021. The National Meteorological Center issued an orange alert on 28 December, the first such alert in China in nearly 5 years. Temperatures decreased

sharply across the whole EC, accompanied by gusts of force 7–9 and heavy snow in several areas, and the 0 °C line reached Guangzhou (approximately 23° N). The SAT decreased by more than 12 °C, covering an area of 1750 000 km^2. A new round of cold air began on 5 January, and the SAT in EC decreased again by 6 °C–10 °C, which induced the minimum SAT at 60 meteorological observation stations to break their historical record lows (Zheng *et al* 2021).

Since the late 1990s, the mid-high latitudes of Eurasia has shown a cooling trend, with extreme cold events occurring frequently (Liu *et al* 2012, Cohen *et al* 2014, Ma and Zhu 2020). However, the Arctic sea ice melted rapidly, and the SAT in the Arctic increased rapidly at a rate approximately 2–3 times that of the global average, which is referred to as 'Arctic amplification' (Francis and Vavrus 2012, Feng and Wu 2015, Gao *et al* 2015). Arctic warming is particularly evident near the Barents–Kara Sea and is in sharp contrast to the cooling in Siberia, which forms the pattern termed 'Warm Arctic-Cold Siberia' (WACS) or 'Warm Arctic-Cold Eurasia' (Inoue *et al* 2012, Kim *et al* 2014, Wang and Liu 2016). The existence of WACS could also be detected in SAT anomalies, 1000–500 hPa thickness fields and middle troposphere temperatures (Overland and Wang 2010, He *et al* 2020). In addition to the winter mean SAT that many previous studies have been concerned about, the first empirical orthogonal function (EOF) of daily SAT in winter also diagnosed the WACS signal on a daily time scale (figure S1(a) (available online at stacks.iop.org/ERL/16/094040/mmedia)). As described by earlier studies, this pattern did not appear in the first EOF of the seasonal mean SAT during 1979–1998, but became dominant since the late 1990s (Tyrlis *et al* 2020). However, the first EOF of daily SAT during the two subperiods (i.e. 1979–1998 and 1999–2018) was robustly characterized by the WACS pattern (figures S1(c)–(f)), indicating the necessity to explore WACS pattern both on the daily scale and seasonal mean scale. The sharp contrast between the warming Barents–Kara Sea and the cooling Siberia could inevitably lead to a reduction in the large-scale meridional temperature gradient at mid-high latitudes, which weakened the atmospheric baroclinicity (Outten and Esau 2012, Luo *et al* 2016, Tao *et al* 2019), and influence the upper-level jet stream and Rossby wave activities (King *et al* 2016, Zhang *et al* 2016). As mentioned above, much evidence implies that extreme cold events in EC were closely related to atmospheric anomalies at mid-high latitudes, and the focus was basically on the impacts of Arctic warming on mid-latitude climate change (Johnson *et al* 2018, Ma *et al* 2018). This raised the question of whether the 2020/21 record-breaking cold waves in EC were tied to the co-occurrence of warm Arctic and cold Siberia on the perspective of a synoptic scale, and how the WACS pattern affected the source, accumulation and path of cold air. In this study, we also attempt to discover the impacts of the WACS (i.e. a holistic pattern) on cold events in EC (the south of 40° N) on an interannual-decadal time scale.

2. Data and methods

2.1. Data description

Daily meteorological data for the winter of 1979–2018 were obtained from NCEP/NCAR Reanalysis datasets (2.5° × 2.5°), including the air temperatures from the surface to 200 hPa and at 10 hPa, geopotential height at 500 hPa, and zonal winds at 200 hPa (Kalnay *et al* 1996), to reveal the linkages on the synoptic scale. The same daily meteorological data in the winter of 2020 were also used to explore variations in the 2020/21 record-breaking cold wave. Monthly mean meteorological data, including air temperature and zonal winds from the surface to 200 hPa for the winter of 1979–2018, were also acquired from NCEP/NCAR Reanalysis datasets (Kalnay *et al* 1996). The monthly mean minimum and maximum temperatures at 2 m for the winter of 1979–2018 were obtained from NCEP-DOE Reanalysis 2 with a Gaussian grid (Kanamitsu *et al* 2002). The simulation data of 46 historical experimental models (table S2) from the sixth phase of the coupled model intercomparison project (CMIP6) for the winter of 1979–2013 were used to verify our conclusion (Eyring *et al* 2016). Historical experiments were conducted to simulate historical climate driven by observational and time-varying external forcing, reflecting climate variability and trends.

2.2. Methods

The daily meteorological data were processed by removing the climatological mean annual cycle. The climatological mean annual cycle was defined as the 40 year (1979–2018) average of the 30 d running mean daily meteorological variables. The daily SAT with removal of the climatological mean annual cycle was defined as RSAT. The linear trends of winter mean meteorological variables were removed. The winter mean SAT after detrending was defined as DSAT.

The atmospheric baroclinicity is expressed by the Eady growth rate, which is a measure of baroclinic instability through the vertical gradient in the horizontal wind (Eady 1949, Bretherton 1966). The function is given by $\sigma_E = 0.3098\frac{|f|\left|\frac{\partial u(z)}{\partial z}\right|}{N}$ (Vallis 2006), where f is the Coriolis parameter, u (z) is the vertical profile of the westerly winds, z is the vertical coordinate, and N is the buoyancy frequency ($N^2 = \frac{g}{\theta}\frac{\partial\theta}{\partial z}$, in which g and θ are gravitational acceleration and potential temperature, respectively).

3. WACS enhanced cold waves

3.1. Relationships on the synoptic scale

Two continuous processes of cold air conjointly contributed to the record-breaking cold wave in the winter of 2020/21. On latter half of December, the SAT in mid-high latitudes persistently showed a significant pattern of WACS. The RSAT difference between the Barents–Kara Sea and Siberia (Barents–Kara Sea minus Siberia) reached 10 °C on 26 December (figure 1(a)), which strongly weakened the large-scale temperature gradient. Subsequently, the first cold air fully invaded EC during 28–31 December (figure 1(b)) and brought a −10 °C SAT anomaly with respect to the climatological mean annual cycle (figure 1(c)). As mentioned above, the observed SAT in EC decreased by 10 °C–12°C (Zheng *et al* 2021). With the warming areas of Arctic and cooling areas of Siberia further expanding to the southeast, the WACS pattern became more pronounced. On 3 January 2021, the RSAT difference between the Barents–Kara Sea and Siberia reached 20 °C, the peak of the 2020/21 winter (figure 1(e)), further weakening the temperature gradient at mid-high latitudes. After 4 d, EC experienced an even more heavy response of the −10.9 °C anomaly during the second cold air outbreak (figure 1(g)), with an observed SAT decrease of more than 8 °C covering an area of 2500 000 km^2 and a record-breaking minimum SAT at 60 stations.

In the following February of the same winter, EC began a record-breaking warming, with observed SAT rebounding by 6 °C–10 °C. An 'Cold Arctic-Warm Eurasia' pattern (i.e. the opposite pattern of WACS) was found as a significant precursory signal, with a −8.8 °C RSAT difference between the Barents–Kara Sea and Siberia on 17 February (figure S2). Subsequently, EC exhibited the most intense warming on 21 February, with a 7.5 °C increase compared to the climatological mean annual cycle (figure S2(g)), causing 494 meteorological observation stations to exceed the historical high record for the same period, and these stations were mainly concentrated in North and Central China. Regardless of the cold or warm events, the strong WACS or strong antiphase WACS patterns had been observed prior to them, indicating that the potential relationship between SAT anomalies in EC and the WACS pattern was robust. These two extreme weather processes were repeatedly analyzed with the SAT that removed the annual cycle of the current year, and identical results were obtained (figure not shown).

The area-averaged RSAT over the Barents–Kara Sea (65°–85° N, 30°–90° E; see box in figure 1) and Siberia (40°–60° N, 60°–120° E; see box in figure 1) were calculated as the $RSAT_{WA}$ and $RSAT_{CS}$ index, and the difference between them was defined as the $RSAT_{WACS}$ index ($RSAT_{WA}$ minus $RSAT_{CS}$) to represent the entire variation in the WACS pattern. The RSAT in EC ($RSAT_{EC}$), which lagged about 4 d (the positive lag meant that the $RSAT_{EC}$ lagged $RSAT_{WACS}$), exhibited the strongest correlation with $RSAT_{WACS}$ (figure 2). This number of lag days is approximately a quarter of the average cycle for WACS (table S1). During the cold air outbreak in January and the warming event in February, the maximum response in EC both occurred 4 d after the $RSAT_{WACS}$ arrived at the largest point (figure 1(e); figure S1(g)). The highest correlation coefficient reached −0.44 (above the 99% confidence level), which was significantly higher than that between $RSAT_{WA}$ and $RSAT_{EC}$ (–0.27, insignificant at the 99% confidence level), suggesting that the cold events over EC were related to the WACS pattern instead of the warm Arctic alone. Furthermore, the lead-lag correlation coefficient between $RSAT_{CS}$ and $RSAT_{WA}$ reached its maximum on day 0, indicating the synchronical changes between them, and it also suggested the rationality to analyze the overall effect of the large-scale temperature gradient changes associated with the WACS pattern.

After removing the climatological mean annual cycle from the daily SAT during winter, all days in 1979–2018 were divided into four categories based on the $RSAT_{WA}$ and $RSAT_{CS}$: WACS ($RSAT_{WA} > 0$, $RSAT_{CS} < 0$; WACS), Cold Arctic-Warm Siberia ($RSAT_{WA} < 0$, $RSAT_{CS} > 0$; CAWS), Cold Arctic-Cold Siberia ($RSAT_{WA} < 0$, $RSAT_{CS} < 0$; CACS) and Warm Arctic-Warm Siberia ($RSAT_{WA} > 0$, $RSAT_{CS} > 0$; WAWS). The WACS pattern and its opposite phase (i.e. CAWS) represented reverse SAT anomalies in the Barents–Kara Sea and Siberia, and the other two represented changes in the same direction (i.e. WAWS and CACS). According to the variation in the lead-lag correlation between $RSAT_{WACS}$ and $RSAT_{EC}$ in figure 2, the RSAT with a four-day lag for these four categories was composited. Corresponding to the WACS pattern, with a weaker meridional temperature gradient, the $RSAT_{EC}$ significantly decreased with a −2.8 °C anomaly and extended to the southernmost region of China (figure 3(a)), which was coincided with the 2020/21 record-breaking cold events (figures 1(c) and (g)). In the CAWS phase, the $RSAT_{EC}$ exhibited the opposite responses with a significant warming of 2.5 °C (figure 3(b)). The impacts of the CAWS phase could also affect the southernmost region of China and very likely contributed to the extreme warm event in February (figure S2). When the Barents–Kara Sea and Siberia cooled or warmed uniformly, EC had the same change in SAT but with much weaker responses (–0.9 °C and 1.0 °C, respectively; figures 3(c) and (d)). In addition, the spatial range of responses was much smaller than that in figures 3(a) and (b). Thus, under the pattern of Siberian cooling (warming), if warming (cooling) signals occurred in the Barents–Kara Sea, the cold (warm) events in EC would be greatly strengthened and expanded.

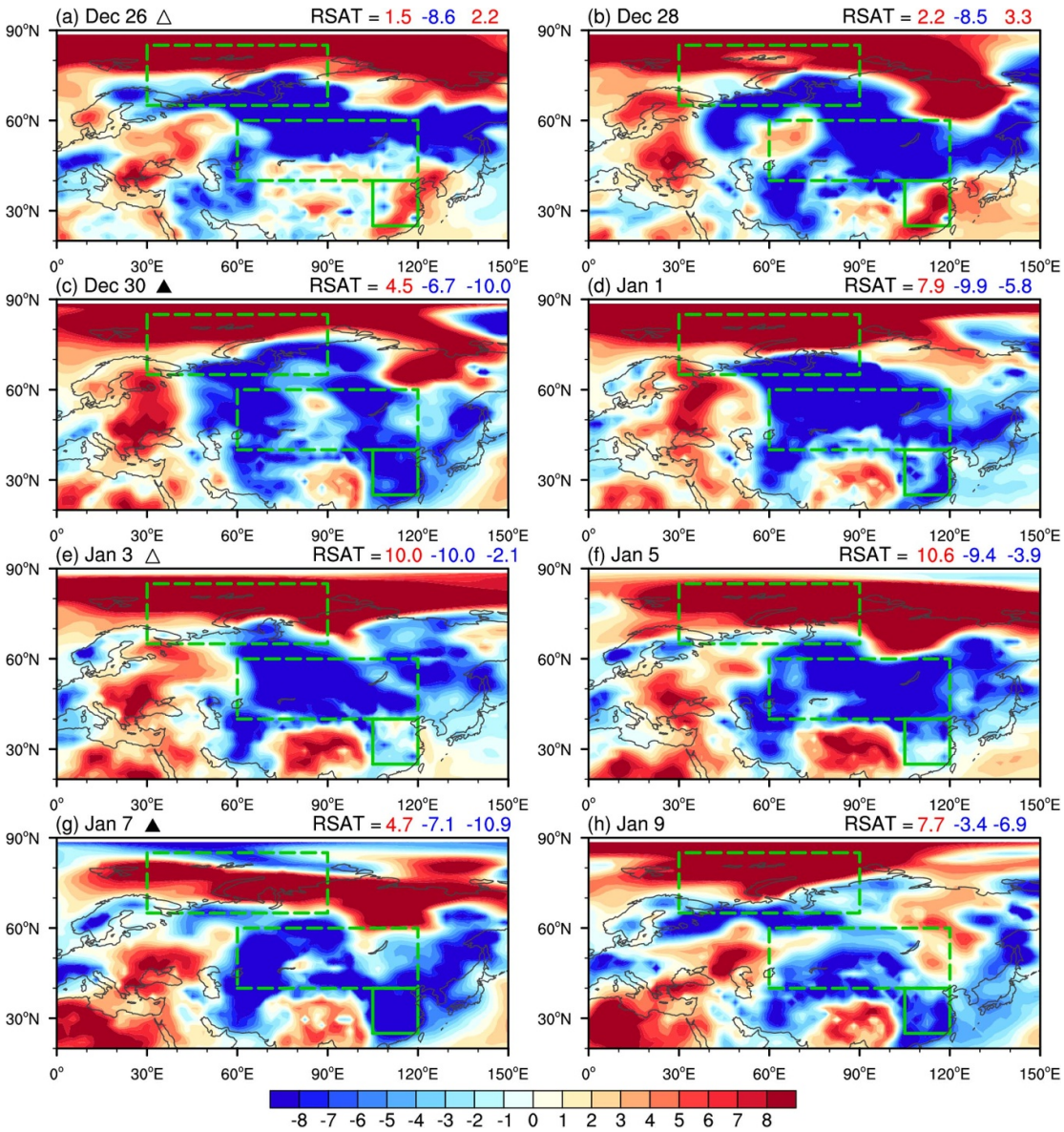

Figure 1. Evolution of daily RSAT (unit: °C) from 26 December 2020 to 9 January 2021. The values of area-averaged RSAT in the Arctic, Siberia and the east of China are listed in each panel, with red for positive anomalies and blue for negative anomalies. The climatological mean annual cycle is removed. The most significant RSAT days in east of China are marked by filled triangles (on 30 December and 7 January), and their lead 4 d (Daylead4) are marked by hollow triangles (on 26 December and 3 January). The green solid box represents the east of China (25°–40° N, 105°–120° E), and two green dotted boxes represent the areas of the Arctic (65°–85° N, 30°–90° E) and Siberia (40°–60° N, 60°–120° E).

Furthermore, similar composites were conducted for 1979–1995, 1996–2011 and 2012–2018, in which trends of WACS varied. During 1996–2011, when the trend of Arctic warming and Eurasian cooling was most pronounced, $RSAT_{EC}$ responded −3.0 °C to WACS pattern (figure 3(e)). While in the most recent decade, it is evident that the impacts of the WACS pattern on the variation in SAT over EC strengthened (i.e. $RSAT_{EC} = -3.7$ °C; figure 3(e)). The response of $RSAT_{EC}$ was consistent and robust in the three period, but with differences in intensity. Several studies pointed out that the winter mean cooling trend in Siberia disappeared over the past decade (Blackport and Screen 2020; Van Oldenborgh *et al* 2019). However, this did not affect the relationship between WACS and $RSAT_{EC}$ on the daily scale, and even showed an enhancement, indicating potential availability to improve the mid-range forecast of extreme SAT anomalies in EC.

3.2. Associated atmospheric anomalies

In this section, the days with $|RSAT_{WACS}|$ > one standard deviation (i.e. $RSAT_{WACS}$ > 1 standard deviation meant the WACS days, and $RSAT_{WACS}$ < minus one standard deviation meant the CAWS days), which defined as day 0, were selected for composite. The relevant composite results of RSAT and associated variables (the WACS days minus the CAWS days) represented the significant WACS pattern and its characteristics (figures 4(c) and (d)). Meanwhile,

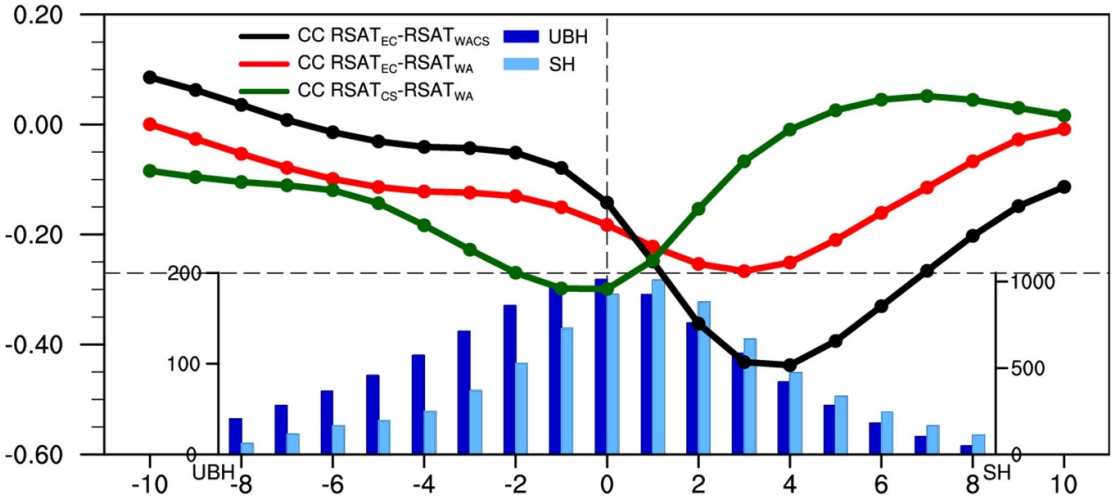

Figure 2. Lead-lag correlation coefficients of $RSAT_{EC}$ relative to the winter daily $RSAT_{WACS}$ (black) and $RSAT_{WA}$ (red), and $RSAT_{CS}$ relative to the winter daily $RSAT_{WA}$ (green). The positive lag means that $RSAT_{EC}$ lagged $RSAT_{WACS}$ in the black line, $RSAT_{EC}$ lagged $RSAT_{WA}$ in the red line, and $RSAT_{CS}$ lagged $RSAT_{WA}$ in the green line. Daily lead-lag composite evolution in the anomalies of the UBH (blue bar) and SH (light blue bar) under the pattern of 'Warm Arctic-Cold Eurasia'. The area-averaged geopotential height at 500 hPa over the Ural Mountain (55°–70° N, 50°–100° E) and sea level pressure over central Siberia (40°–60° N, 80°–120° E) are defined as the anomalies of the UBH (unit: m) and SH (unit: pascals), respectively. The lead-lag correlation coefficients and variations are calculated as the 40 year (1979–2018) average of the correlation coefficient and variation in each year. The climatological mean annual cycle is removed. The horizontal dashed line indicates the correlation coefficient was above the 99% confidence level, and the vertical dash line indicates the day 0.

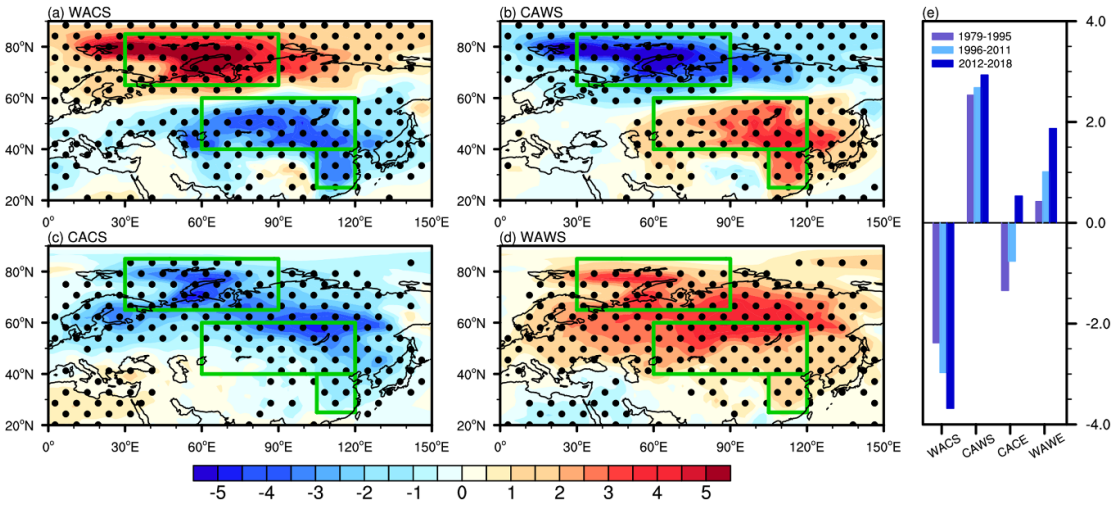

Figure 3. Composite of Daylag4 RSAT (unit: °C) under the pattern of (a) 'Warm Arctic-Cold Siberia', (b) Cold Arctic-Warm Siberia, (c) Cold Arctic-Warm Siberia, and (d) Warm Arctic-Warm Siberia. (e) The composite of Daylag4 $RSAT_{EC}$ under the four patterns during 1979–1995 (purple), 1996–2011 (light blue) and 2012–2018 (blue). The climatological mean annual cycle is removed. The green boxes represent the locations of the Arctic, Siberia and the east of China. Black dots indicate that the composite results were above the 95% confidence level.

DayleadN and DaylagN referred to N days before and after day 0, respectively. For example, Daylag4 indicated the 4 d after the significant WACS pattern, and the composite of associated anomalous circulations and $RSAT_{EC}$ in figures 4(e) and (f) was as the responses to the co-occurrence of Arctic warming and Siberian cooling. On Daylead4, the WACS pattern had already been observed in air temperature both near the surface (figure 4(a), figure S3(a)) and in the upper troposphere (figure S4(a)). Over time, the WACS pattern reached its strongest value on day 0 (figure 4(c)), with temperature anomalies extending to 250 hPa and moving more south (figure S4(c)). Compared with the climatology, it could be more clearly recognized that the anomalies of meridional temperature gradient were further reinforced and expanded (figures 4(c) and S3(a)). The temperature anomalies in the Barents–Kara Sea and Siberia from lower to upper troposphere represented that the meridional temperature gradient between middle and high latitudes decreased (figure 4(b)), which resulted in the significant weakening of atmospheric baroclinicity (figure S4(d)) and westerly jet at around 60° N relative to the climate mean (figures 4(d)

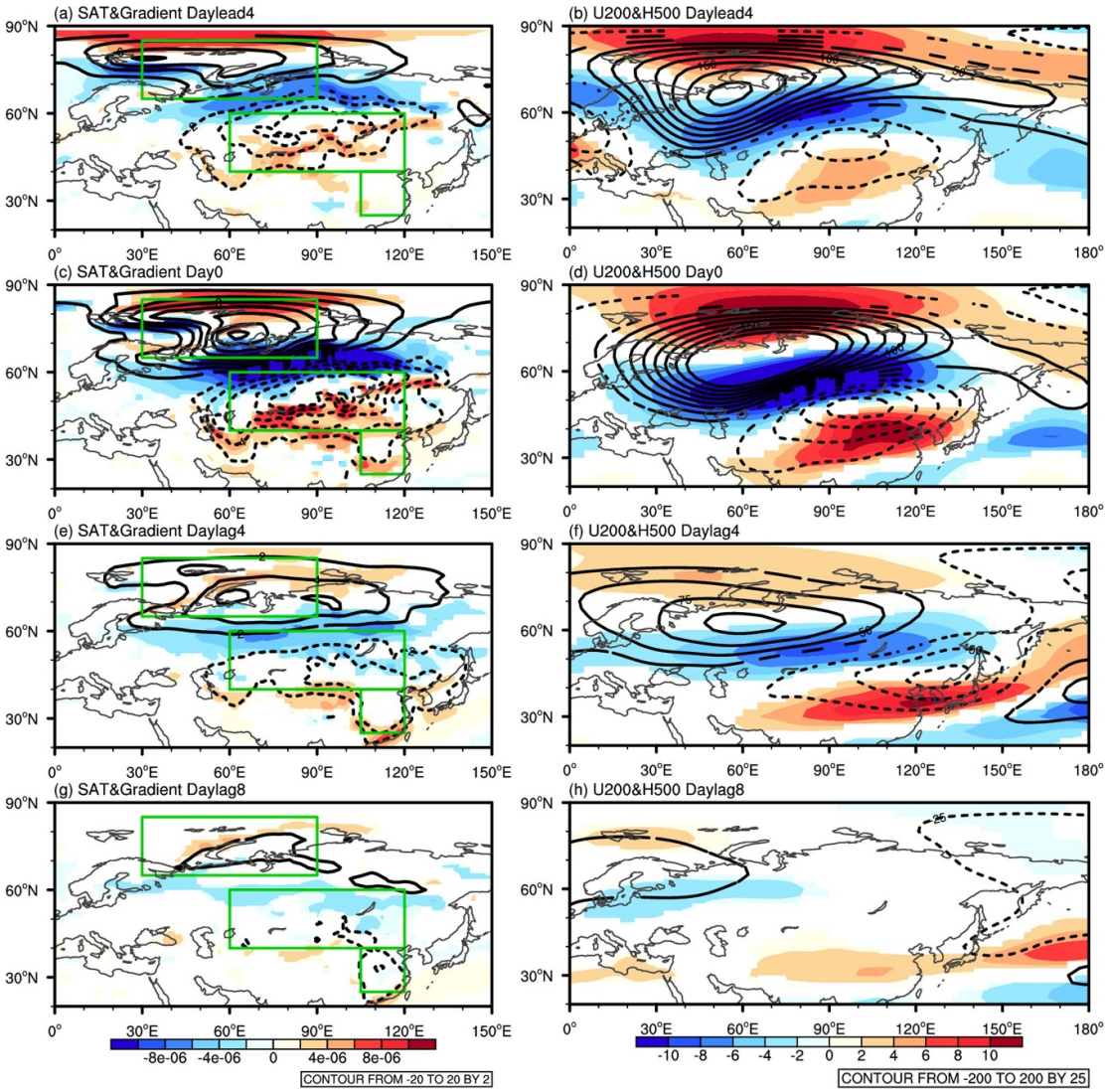

Figure 4. Daily lead-lag composite evolution of (a), (c), (e), (g) RSAT (contours; unit: °C), meridional temperature gradient (shading; unit: °C km^{-1}), (b), (d), (f), (h) geopotential height at 500 hPa (contours; unit: m) and zonal wind at 200 hPa (shading; unit: m s^{-1}) under the pattern of 'Warm Arctic-Cold Siberia'. The climatological mean annual cycle of the daily meteorological data is removed. Shading and contours denote significant composite results above the 95% confidence level. The green boxes represent the locations of the Arctic, Siberia and the east of China.

and S3(b)). These changes in mean flow provided favorable conditions for the enhancement and maintenance of the UBH (Luo *et al* 2017), and thus, the UBH achieved its maximum amplitudes on day 0 (figure 4(d); figure 2). It seemed that $RSAT_{WA}$, $RSAT_{CS}$, and the UBH appeared to peak at the same time. The extremely strong UBH usually led to a strengthening SH (Ma and Zhu 2019), which reached the strongest value on Daylag1 (figure 2), and accumulated and guided cold air southward into China through cold air advection (figure S5(b)). When the UBH collapsed on Daylag4, the cold air behind the deep trough over Lake Baikal moved southward in a large way (figure 4(f)), resulting in an outbreak of cold air across EC that even affected the southernmost areas (figures 4(e) and S5(c)). While the intensity of warm and cold centers became weaker and moved southeastward, similarly in the upper troposphere (figures 4(e) and S4(e)). On Daylag8, i.e. 4 d after the cold event outbreak, the WACS pattern became no longer significant, and the meridional temperature gradient and baroclinicity gradually returned to normal (figures S4(g) and (h)). The crucial UBH and SH anomalies also retreated westward and disappeared, and the trough moved eastward into the East China sea (figure 4(h)).

During the 2020/21 massive and continuous cold event in EC, the aforementioned atmospheric anomalies associated with the WACS pattern could be distinctly observed (figure S6). Accompanied by a significant pattern of WACS with a weakening temperature gradient (figures 1(a) and (b)), the UBH maintained and strengthened steadily before the first cold air process (figure S6(a)), which transported and accumulated cold air behind the deep trough over Lake Baikal. The westerly jet stream weakened

considerably, providing an unobstructed path for the southward transport of cold air. Starting on 28 December, the cold air expanded southward constantly into EC (figures S6(b) and (c)). Meanwhile, as the WACS pattern became more pronounced and the temperature gradient further weakened (figures 1(e) and (f)), the UBH remained stable, and a new deep trough was incubated and enhanced with a southeastward movement (figures S6(d) and (e)). A new round of cold air invaded EC from 5 January under the combination of abnormal circulations (figures 1(e)–(h); figures S6(f) and (g)). With the collapse of the UBH retreating westward and the complete release of cold air behind the trough, the cold event tended to end on 9 January (figure S6(h)). Furthermore, the record-breaking warming event in February of the same winter was accompanied by an opposite pattern of the WACS with contrary atmospheric anomalies (figures S2 and S7). The negative height anomaly maintained and developed near the Ural Mountain, which impeded the formation of the UBH. The abnormal southerly winds brought warm and humid air into EC, causing significant warming on 21 February (figure S5(g)).

4. Interannual-decadal linkages and physical mechanisms

In numerous studies, the pattern of WACS was mainly diagnosed from different winter-mean variables and showed interannual-decadal variation and trend changes (Overland and Wang 2010, He *et al* 2020). In this study, we also further explored the interannual-decadal relationship between the WACS pattern and cold events in EC by using the winter monthly mean data. Similarly, the area-averaged DSAT over the Barents–Kara Sea and Siberia were calculated as the $DSAT_{WA}$ and $DSAT_{CS}$ indices, and the difference between them was defined as the $DSAT_{WACS}$ index ($DSAT_{WA}$ minus $DSAT_{CS}$). All years in 1979–2018 were also divided into four categories based on the $DSAT_{WA}$ and $DSAT_{CS}$. The difference between WACS years ($DSAT_{WA} > 0$, $DSAT_{CS} < 0$) and CAWS years ($DSAT_{WA} < 0$, $DSAT_{CS} > 0$) was composited to highlight the effect of the WACS pattern on the climate anomaly in EC. The winter mean climate throughout EC responded a significant cooling to the WACS pattern (figure 5(a)). Among the other temperature variables, the area-averaged composite of minimum and maximum SAT in EC decreased by 1.5 °C and 2.0 °C, respectively, and the area-averaged composite of the number of extreme cold days (the minimum SAT below the 5% quantile) in EC increased considerably by 3.4 d. The responses of these variables strongly verified that the WACS pattern contributed to a cold winter in EC on the seasonal mean scale. With the meridional temperature gradient shrinking significantly from the surface to middle troposphere (figure 5(b), figure S8(a)), the atmospheric baroclinicity weakened significantly (figure S8(b)), which was conducive to the development and maintenance of the UBH and Baikal deep trough, thus causing a cold winter to occur. However, when the Barents–Kara Sea and Siberia were warming or cooling together, EC would not show a significant anomaly in winter-mean (figures S9(c) and (d)). Only with opposite SAT anomaly signals appearing would EC respond to a cold winter or warm winter (figures S9(a) and (b)), indicating that the connection between winter-mean SAT anomalies in EC and the WACS pattern performed stronger.

The correlation coefficient between winter-mean $DSAT_{WACS}$ and $DSAT_{EC}$ was −0.77 and was significant at the 99% confidence level (figure 5(c)). After removing the signal of the El Niño-Southern Oscillation (ENSO) by subtracting linear regression of SAT onto the ENSO from SAT, so as to exclude the role of ENSO in the relationship, the correlation coefficient remained at −0.75, indicating that this relationship was independent of the tropical signal. As revealed by Ma and Zhu (2019), the warm Arctic has significantly contributed to the frequent extreme cold events in EC during recent years. However, the response of winter-mean SAT in EC ($DSAT_{EC}$) to $DSAT_{WA}$ was much weaker than that to $DSAT_{WACS}$ (figure S10(a)) and was insignificant in Northeast China. The correlation coefficient between $DSAT_{WA}$ and $DSAT_{EC}$ was −0.51 and significantly weaker than that with $DSAT_{WACS}$ (figure 5(c)). That is, even on the interannual-decadal time scale, the joint impact of a warm Arctic and cold Siberia on cold events in EC was significantly stronger than that of only considering the Arctic warming signal, which was consistent with the result on the synoptic scale. The relationship between the WACS pattern and $DSAT_{EC}$, as well as that between Arctic warming and $DSAT_{EC}$, was further verified by extensive multimodel CMIP6 simulations. A total of 44 out of 46 models showed a statistically significant negative correlation between $DSAT_{WACS}$ and $DSAT_{EC}$, which meant that the relationship that WACS pattern enhanced the cold winter in EC could also be detected in CMIP6 simulations. Furthermore, all models revealed a higher negative correlation between $DSAT_{WACS}$ and $DSAT_{EC}$ than between $DSAT_{WA}$ and $DSAT_{EC}$ (figure 5(d)). The multimodel ensemble mean correlation coefficient was −0.59 (above the 99% confidence level) between $DSAT_{WACS}$ and $DSAT_{EC}$ and −0.28 (insignificant) between $DSAT_{WA}$ and $DSAT_{EC}$ (figure 5(d)). The results from CMIP6 datasets supported the aforementioned speculation that the temperature contrast between the Arctic and Siberia was a more effective signal that influenced temperature over EC.

5. Conclusion and discussion

Both the daily and interannual-decadal linkages between the winter SAT anomalies in EC and the

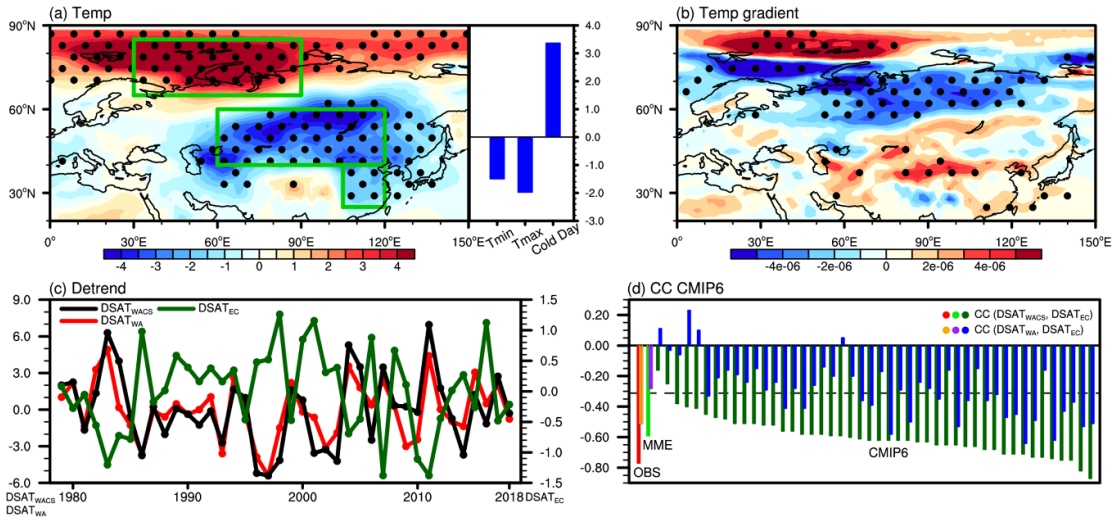

Figure 5. Composite analysis of winter mean (a) SAT (shading; unit: °C), minimum SAT (bar; unit: °C), maximum SAT (bar; unit: °C), the number of cold days (bar) and (b) meridional SAT gradient (unit: °C km^{-1}) under the pattern of 'Warm Arctic-Cold Siberia'. The linear trend is removed. (c) Temporal evolution of winter mean $DSAT_{WACS}$, $DSAT_{WA}$, and $DSAT_{EC}$. (d) Correlation coefficients between winter mean $DSAT_{EC}$ and $DSAT_{WACS}$ (green) and between $DSAT_{EC}$ and $DSAT_{WA}$ (blue) in the 46 CMIP6 simulations. Red and orange bars show the correlation coefficients of reanalyzed data. Light green and purple bars denote the multimodel ensemble mean correlation coefficients. Black dots in (a) and (b) indicate the composite results were above the 95% confidence level. The dashed line in (d) indicates the correlation coefficients were above the 95% confidence level.

temperature contrast at mid-high latitudes (Arctic minus Siberia) were explored in this study. More importantly, the record-breaking cold waves and warm events in the winter of 2020 could be explained by the 'Warm Arctic-Cold Siberia' pattern and its opposite pattern to a large extent. The WACS pattern as a precursory signal significantly enhanced the cold waves in EC and tended to precede the strongest $RSAT_{EC}$ response by approximately 4 d. With the meridional temperature gradient at mid-high latitudes shrinking, the atmospheric baroclinicity weakened correspondingly, which led to an extremely strong UBH and deep trough over Lake Baikal, thus transporting persistent cold air into EC through the strengthened northerly wind. The record-breaking cold wave in winter 2020/21 was accompanied by a significant WACS signal and such atmospheric anomalies. After the RSAT difference between the Barents–Kara Sea and Siberia reaching its largest in winter 2020/21 of 20 °C on 3 January, the observed SAT significantly decreased by 6 °C–10 °C. Furthermore, the February record-breaking warming event in the same winter was accompanied by an antiphase of the WACS pattern and opposite atmospheric anomalies. Regarding the interannual variation, the aforementioned relationship between the WACS pattern and the cold winter in EC existed and even performed stronger both in the observations and simulation data of CMIP6. However, when the SAT anomalies in the Barents–Kara Sea and Siberia changed in the same direction, EC would not respond significantly in winter, supporting our view that the temperature contrast between the Arctic and Siberia was a more effective signal influencing temperature over EC. From the daily lead-lag relationship, it seemed that the simultaneous variation of the WACS pattern and UBH caused the SH to reach its strongest extent on Daylag1, thus further affecting the cold wave in EC. However, the physical mechanism between them has not been clearly studied and deserves further attention and exploration.

In addition to the effects of the near-surface and troposphere, it is well documented that stratospheric sudden warming (SSW) has a significant impact on cold events in EC (Li *et al* 2010). The SSW was generally characterized by the phenomenon that the meridional gradient of zonal mean temperature from 60° N to the polar region reversed in the stratosphere at 10 hPa or below. Li *et al* (2010) pointed out that after the occurrence of a strong SSW, the anomalous circulation in the stratosphere would form a negative Arctic Oscillation phase between mid-high latitudes and would spread downward to the troposphere, which strengthened the SH, deepened the East Asian trough and resulted in abnormally cold events in EC. Here, we calculated the daily meridional gradient of zonal mean temperature from 60° N to the polar region at 10 hPa in the winter of 2020 to show the evolution of SSW. Indeed, this reverse meridional temperature gradient at 10 hPa could be detected before the cold air outbreak on 5 January (figure S11) and must have contributed to the 2020/21 record-breaking cold events. However, among the four processes of cold air activities (i.e. 12–15 and 28–31 December, 5–8 and 14–17 January) in the

winter of 2020, only two SSWs occurred (i.e. 2–7 and 14–16 January; figure S11). The emergence of these two SSWs was not as leading as many studies have suggested (Choi *et al* 2021, Lu *et al* 2021). In contrast, positive peaks of $RSAT_{WACS}$ were observed during all four cold air events. Likewise, negative values of $RSAT_{WACS}$ continued from 26 January to 20 February, and the 'Cold Arctic-Warm Siberia' pattern significantly facilitated the record-breaking warm event in the same winter. It looks like the impacts of surface signals appeared to be more stable. Furthermore, SSW events could also relate to the weaker states of the polar vortex (Hoshi *et al* 2019, Baldwin *et al* 2021). Previous studies have shown that low sea ice conditions can weaken the polar vortex mean state, reinforce the SH through stratosphere-troposphere coupling, and thus advection leads to cold extremes in eastern Asia (Kim *et al* 2014, Sun *et al* 2015, Labe *et al* 2019). Therefore, the synergetic mechanisms between SSW and the WACS pattern and the role of stratosphere-troposphere coupling in strengthening the WACS pattern in 2020 winter are still open and worthy questions.

From the view of winter mean, EC did not respond a significant cooling or warming in winter 2020/21, with a temperature anomaly of 0.05 °C after detrending (figure S12), which was very close to 0 °C. However, the extreme cold events and extreme warm events happened in EC on a synoptic scale. The $DSAT_{WACS}$ showed an insignificant opposite phase of WACS (i.e. CAWS) in winter mean of 2020/21 (figure S12), which concealed the shift of $RSAT_{WACS}$ on the synoptic scale (figure S11). The record-breaking cold and warm events in the same 2020/21 winter implied large variability of SAT in EC, which has always caused problems for decision-making and disaster prevention. This large SAT variability over EC is likely a result from the dynamic effects of rapid Arctic warming and the thermodynamic effects of global warming (Ma *et al* 2018). The $RSAT_{WACS}$ in winter 2020/21 was positive before mid-January 2021 and then turned negative, indicating that the WACS pattern also contributed to the large SAT variability or subseasonal SAT variability over EC. The reasons for the subseasonal shift of WACS in winter 2020/21 deserve further study. As to the preceding climate drivers, Zheng *et al* (2021) illustrated that the moderate La Niña event that began in August 2020 provided an indispensable background for the extreme cold winter in 2020/21. In addition, the extent of Arctic sea ice in autumn 2020 shrank to the second lowest since modern record-keeping began in the late 1970s (https://nsidc.org/arcticseaicenews/) and possibly contributed to the cold events (Zheng *et al* 2021). However, the synergistic effect of decreased Arctic sea ice and a cold tropical Pacific in 2020 and their contributions are still unclear and need further observational and numerical research.

Data availability statement

Daily temperatures at 2 m can be obtained from https://www.psl.noaa.gov/cgi-bin/db_search/DBListFiles.pl?did=198&tid=94423&vid=3083. Daily air temperatures from 1000 to 200 hPa and at 10 hPa can be obtained from https://www.psl.noaa.gov/cgi-bin/db_search/DBListFiles.pl?did=198&tid=94422&vid=4984. Daily geopotential height at 500 hPa can be obtained from https://www.psl.noaa.gov/cgi-bin/db_search/DBListFiles.pl?did=198&tid=94422&vid=663. Daily zonal winds at 200 hPa can be obtained from https://www.psl.noaa.gov/cgi-bin/db_search/DBListFiles.pl?did=198&tid=94422&vid=666. Monthly mean temperatures at 2 m and monthly mean minimum and maximum temperatures can be obtained from https://www.psl.noaa.gov/data/gridded/data.ncep.reanalysis2.gaussian.html. Monthly mean zonal winds from 1000 to 200 hPa can be obtained from https://www.psl.noaa.gov/data/gridded/data.ncep.reanalysis.pressure.html. The simulation data of 46 CMIP6 models are available from https://esgf-node.llnl.gov/search/cmip6/.

Acknowledgments

This research is supported by the National Natural Science Foundation of China (Grant Nos. 42088101, 42025502 and 41991283).

Author contributions

Wang H J and Yin Z C designed the research. Yin Z C and Zhang Y J performed research. Zhang Y J prepared the manuscript with contributions from all co-authors.

Conflict of interest

The authors declare no conflict of interest.

ORCID iD

Shengping He https://orcid.org/0000-0003-4245-357X

References

Baldwin M P *et al* 2021 Sudden stratospheric warmings *Rev. Geophys.* **59** e2020RG000708

Blackport R and Screen J A 2020 Weakened evidence for mid-latitude impacts of Arctic warming *Nat. Clim. Change* **10** 1065–6

Bretherton F 1966 Critical layer instability in baroclinic flows *Q. J. Roy. Meteorol. Soc.* **92** 325–34

Choi H, Kim J H, Kim B M and Kim S J 2021 Observational evidence of distinguishable weather patterns for three types of sudden stratospheric warming during northern winter *Front. Earth Sci.* **9** 625868

Cohen J *et al* 2014 Recent arctic amplification and extreme mid-latitude weather *Nat. Geosci.* **7** 627–37

Ding T, Gao H and Li X 2020 Increasing occurrence of extreme cold surges in North China during the recent global warming slowdown and the possible linkage to the extreme pressure rises over Siberia *Atmos. Res.* **248** 105198

Ding Y, Wang Z, Song Y and Zhang J 2008 Causes of the unprecedented freezing disaster in January 2008 and its possible association with the global warming *Acta. Meteorol. Sin.* **66** 808–25

Eady E T 1949 Long waves and cyclone waves *Tellus* **1** 33–52

Eyring V *et al* 2016 Overview of the coupled model intercomparison project phase 6 (CMIP6) experimental design and organization *Geosci. Model Dev.* **9** 1937–58

Feng C and Wu B 2015 Enhancement of winter Arctic warming by the Siberian high over the past decade *Atmos. Ocean Sci. Lett.* **8** 257–63

Francis J and Vavrus S 2012 Evidence linking arctic amplification to extreme weather in mid-latitudes *Geophy. Res. Lett.* **39** L06801

Gao Y, Sun J, Li F, He S and Suo L 2015 Arctic sea ice and Eurasian climate: a review *Adv. Atmos. Sci.* **32** 92–114

He S, Xu X, Furevik T and Gao Y 2020 Eurasian cooling linked to the vertical distribution of Arctic warming *Geophy. Res. Lett.* **47** e2020GL087212

Hoshi K, Ukita J, Honda M, Nakamura T, Yamazaki K, Miyoshi Y and Jaiser R 2019 Weak stratospheric polar vortex events modulated by the Arctic sea-ice loss *J. Geophys. Res.* **124** 858–69

Inoue J, Hori M E and Takaya K 2012 The role of Barents-sea ice in the wintertime cyclone track and emergence of a warm-Arctic cold-Siberian anomaly *J. Clim.* **25** 2561–8

Johnson N, Xie S P, Kosaka Y and Li X 2018 Increasing occurrence of cold and warm extremes during the recent global warming slowdown *Nat. Commun.* **9** 1724

Kalnay E *et al* 1996 The NCEP/NCAR 40-year reanalysis project *Bull. Am. Meteorol. Soc.* **77** 437–71

Kanamitsu M, Ebisuzaki W, Woollen J, Yang S-K, Hnilo J and Fiorino M 2002 NCEP-DOE AMIP II reanalysis (R-2) *Bull. Am. Meteorol. Soc.* **83** 1631–44

Kim B M *et al* 2014 Weakening of the stratospheric polar vortex by Arctic sea-ice loss *Nat. Commun.* **5** 4646

King M P, Hell M and Keenlyside N 2016 Investigation of the atmospheric mechanisms related to the autumn sea ice and winter circulation link in the Northern Hemisphere *Clim. Dyn.* **46** 1185–95

Labe Z, Peings Y and Magnusdottir G 2019 The effect of QBO phase on the atmospheric response to projected Arctic sea ice loss in early winter *Geophy. Res. Lett.* **46** 7663–71

Li L, Li C Y, Tan Y K and Chen C H 2010 Stratospheric sudden warming impacts on the weather/climate in China and its role in the influence of ENSO *Chin. J. Geophy.* **53** 1529–42 in Chinese

Liu J, Curry J A, Wang H, Song M and Horton R M 2012 Impact of declining Arctic sea ice on winter snowfall *Proc. Natl Acad. Sci. USA* **109** 4074–9

Lu Q, Rao J, Guo D, Yu M and Yu Y 2021 Downward propagation of sudden stratospheric warming signals and the local environment in the Beijing-Tianjin-Hebei region: a comparative study of the 2018 and 2019 winter cases *Atmos. Res.* **254** 105514

Luo D, Xiao Y, Yao Y, Dai A, Simmonds I and Franzke C L E 2016 Impact of Ural blocking on winter warm Arctic-cold Eurasian anomalies. Part I: blocking-induced amplification *J. Clim.* **29** 3925–47

Luo D, Yao Y, Dai A, Simmonds I and Zhong L 2017 Increased quasi stationarity and persistence of winter Ural blocking and Eurasian extreme cold events in response to arctic warming. part ii: a theoretical explanation *J. Clim.* **30** 3569–87

Luo J, Chen H and Zhou B 2020 Comparison of snowfall variations over china identified from different snowfall/rainfall discrimination methods *J. Meteorol. Res.* **34** 1114–28

Ma S and Zhu C 2019 Extreme cold wave over east asia in January 2016: a possible response to the larger internal atmospheric variability induced by arctic warming *J. Clim.* **32** 1203–16

Ma S and Zhu C 2020 Opposing trends of winter cold extremes over Eastern Eurasia and North America under recent Arctic warming *Adv. Atmos. Sci.* **37** 1417–34

Ma S, Zhu T, Liu B, Zhou T, Ding Y and Orsolini Y J 2018 Polarized response of East Asian winter temperature extremes in the era of Arctic warming *J. Clim.* **31** 5543–57

Outten S D and Esau I 2012 A link between Arctic sea ice and recent cooling trends over Eurasia *Clim. Change* **110** 1069–75

Overland J E and Wang M 2010 Large-scale atmospheric circulation changes associated with the recent loss of Arctic sea ice *Tellus A* **62** 1–9

Sun B, Wang H and Zhou B 2019 Climatic condition and synoptic regimes of two intense snowfall events in eastern china and implications for climate variability *J. Geophys. Res.* **124** 926–41

Sun L, Deser C and Tomas R A 2015 Mechanisms of stratospheric and tropospheric circulation response to projected Arctic sea ice loss *J. Clim.* **28** 7824–45

Tao L, Sun X and Yang X 2019 The asymmetric atmospheric response to the midlatitude North Pacific SST anomalies *J. Geophys. Res.* **124** 9222–40

Tyrlis E, Bader J, Manzini E, Ukita J, Nakamura H and Matei D 2020 On the role of Ural blocking in driving the Warm Arctic-Cold Siberia pattern *Q. J. R. Meteorol. Soc.* **146** 2138–53

Vallis G K 2006 *Atmospheric and Oceanic Dynamics: Fundamentals and Large-Scale Circulation* (Cambridge: Cambridge University Press)

van Oldenborgh G J, Mitchell-Larson E, Vecchi G A, de Vries H, Vautard R and Otto F 2019 Cold waves are getting milder in the northern midlatitudes *Environ. Res. Lett.* **14** 114004

Wang S and Liu J 2016 Delving into the relationship between autumn Arctic sea ice and central-eastern Eurasian winter climate *Atmos. Ocean Sci. Lett.* **9** 366–74

Zhang J, Tian W, Chipperfield M P, Xie F and Huang J 2016 Persistent shift of the Arctic polar vortex towards the Eurasian continent in recent decades *Nat. Clim. Change* **6** 1094–9

Zheng F *et al* 2021 The 2020/21 extremely cold winter in China influenced by the synergistic effect of La Niña and warm Arctic *Adv. Atmos. Sci.* (https://doi.org/10.1007/s00376-021-1033-y)